



OPEN

Low-spin ferric iron in primordial bridgmanite crystallized from a deep magma ocean

Yoshiyuki Okuda^{1,4}, Kenji Ohta¹, Yu Nishihara², Naohisa Hirao³, Tatsuya Wakamatsu¹, Sho Suehiro¹, Saori I. Kawaguchi³ & Yasuo Ohishi³

The crystallization of the magma ocean resulted in the present layered structure of the Earth's mantle. An open question is the electronic spin state of iron in bridgmanite (the most abundant mineral on Earth) crystallized from a deep magma ocean, which has been neglected in the crystallization history of the entire magma ocean. Here, we performed energy-domain synchrotron Mössbauer spectroscopy measurements on two bridgmanite samples synthesized at different pressures using the same starting material ($\text{Mg}_{0.78}\text{Fe}_{0.13}\text{Al}_{0.11}\text{Si}_{0.94}\text{O}_3$). The obtained Mössbauer spectra showed no evidence of low-spin ferric iron (Fe^{3+}) from the bridgmanite sample synthesized at relatively low pressure of 25 gigapascals, while that directly synthesized at a higher pressure of 80 gigapascals contained a relatively large amount. This difference ought to derive from the large kinetic barrier of Fe^{3+} rearranging from pseudo-dodecahedral to octahedral sites with the high-spin to low-spin transition in experiments. Our results indicate a certain amount of low-spin Fe^{3+} in the lower mantle bridgmanite crystallized from an ancient magma ocean. We therefore conclude that primordial bridgmanite with low-spin Fe^{3+} dominated the deeper part of an ancient lower mantle, which would contribute to lower mantle heterogeneity preservation and call for modification of the terrestrial mantle thermal evolution scenarios.

The early state of the Earth's mantle was likely to be fully molten due to the radiogenic, core formation¹, and the widely believed Moon-forming giant impact^{2–4}. The terrestrial deep magma ocean evolved into the present form of the Earth's mantle through core-mantle differentiation, mineral crystallization, and phase changes. High-pressure melting experiments showed that bridgmanite, an iron and aluminium (Fe,Al)-bearing MgSiO_3 perovskite, is the first crystallizing phase for melts created by partial melting of pyrolitic mantle throughout lower mantle pressures^{5,6}. Recent mantle dynamics simulations have shown that primordial bridgmanite-enriched domains⁷ can persist throughout Earth's history if they have a distinct density and viscosity difference from the surroundings^{8,9}. Heterogeneity preservation is meaningful for explaining the observed primordial isotopic fingerprints^{10,11}, and its investigation requires the detailed physicochemical and rheological properties of bridgmanite.

The electronic spin state of iron in bridgmanite controls various physical and chemical properties of the lower mantle, which is the most voluminous and massive layer on Earth. Since the first experimental demonstration by Badro et al.¹², numerous studies have investigated the mechanism of the spin transition of bridgmanite samples with various chemical compositions and its influence on the properties of bridgmanite^{13–29} (see Lin et al.³⁰ for a review). However, whether iron and aluminium (Fe,Al)-bearing bridgmanite undergoes a spin transition in the lower mantle has remained elusive for decades. Those synthesized at relatively low pressure in a multi-anvil apparatus (MA) show no evidence of the spin transition^{13–18}, implying a high-spin Fe throughout the lower mantle, which is consistent with theoretical studies^{31–34}. On the other hand, other experiments showed the spin transition of ferric iron (Fe^{3+}) in octahedral sites (Si sites) of bridgmanite directly transformed at high pressure in a diamond anvil cell (DAC)^{19,24–28} (Fig. 1).

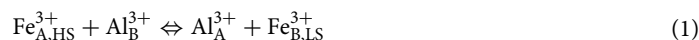
One way to interpret this contradiction is by attributing the invisible spin transition^{13–18} to the difficulty of achieving equilibrium in the site distribution of Fe^{3+} due to the large kinetic barrier of cation exchange^{20–22,25}

¹Department of Earth and Planetary Sciences, Tokyo Institute of Technology, Tokyo 152-8550, Japan. ²Geodynamics Research Center, Ehime University, Ehime 790-8577, Japan. ³Japan Synchrotron Radiation Research Institute, Hyogo 679-5198, Japan. ⁴Present address: Department of Earth and Planetary Sciences, Graduate School of Science, The University of Tokyo, Bunkyo, Tokyo 113-0033, Japan. ✉email: okuda.y@eps.s.u-tokyo.ac.jp

		Polycrystalline								
2nd		Reference	LS-Fe	Method	Reference	LS-Fe	Method	1st		
		Li <i>et al.</i> ²⁶	P	XES	Nishio-Hamane <i>et al.</i> ¹⁶	P	XRD*			
		Fujino <i>et al.</i> ²⁷	P	XES	Catalli <i>et al.</i> ¹⁷	P	T-SMS+XRD			
		Kupenko <i>et al.</i> ²⁸	P	E-SMS	Shim <i>et al.</i> ¹⁸	p [#]	T-SMS+EELS			
		Zhu <i>et al.</i> ²⁹	P	T-SMS+XES	Okuda <i>et al.</i> ¹⁹	P	XRD			
		Fujino <i>et al.</i> ²⁷	N	XRD	Okuda <i>et al.</i> ²⁰	P	XRD			
		Okuda <i>et al.</i> ¹⁵	N	XRD	Dorfinan <i>et al.</i> ²¹	N	E-SMS*			
		Zhu <i>et al.</i> ²⁹	N	XRD						
MA (< 25 GPa)					DAC (> 45 GPa)					
		Ballaran <i>et al.</i> ¹³	N	XRD	Do not exist					
		Potapkin <i>et al.</i> ¹⁴	N	E-SMS						
		Glazyrin <i>et al.</i> ²²		XRD						
		Ismailova <i>et al.</i> ²³	N	XRD						
3rd		Lin <i>et al.</i> ²⁴	N	T-SMS+XES						
		Mao <i>et al.</i> ²⁵	N	T-SMS+XRD						
							4th			

Figure 1. The spin state of Fe in (Fe,Al)-bearing bridgmanite compiled in a two-dimensional diagram with the x-axis the sample synthesis pressure and the y-axis the sample grain size. 1st and 2nd quadrants, studies used a multigrain sample, 3rd and 4th quadrants, studies used a single-crystal sample. 1st and 4th quadrants, sample synthesized in a DAC, 2nd and 3rd quadrants, used a sample pre-synthesized in a MA. Numbers in the table denote the quadrants. *: discussed in Fujino *et al.*²⁰. #: lack clear evidence from their synchrotron Mössbauer spectroscopy (SMS) results but has suggested being present from their Electron Energy-Loss Spectroscopy (EELS) results. *: hiroseite with almandine composition. P present; N no evidence. T- and E-SMS, time- and energy-domain SMS, respectively.

described below, which is suggested to be a plausible process for bridgmanite containing low spin (LS) Fe³⁺ to be generated from initial high spin (HS)²⁰.



However, direct spectroscopic observation of the Fe spin state of (Fe,Al)-bearing MgSiO₃ bridgmanite directly synthesized in a diamond anvil cell (DAC) above 45 GPa is so far limited to 1 report²⁵, making the spin state of Fe in bridgmanite unclear. Examining the aforementioned hypothesis is of great importance for determining the spin state of primordial bridgmanite crystallized from an ancient deep magma ocean and hence its thermal evolution because the proposed scenarios of magma ocean crystallization lack information on the spin state of bridgmanite and its effect^{35–37}.

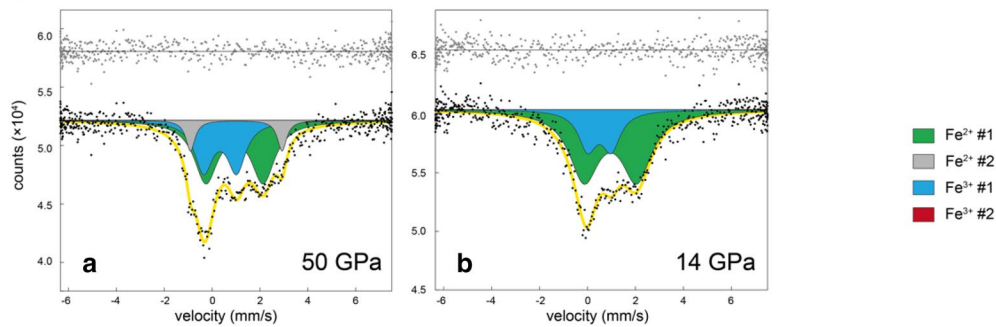
Here, we designed a comparative experiment on two different bridgmanite samples utilizing room-*T* energy-domain SMS combined with a DAC technique that is best suited for the analysis of iron distributions between individual crystal sites in bridgmanite and its Fe³⁺ content and electronic states at high pressures^{14,21,38}. The bridgmanite samples were synthesized from the same gel starting material with a chemical composition of Mg_{0.78(3)}Fe_{0.13(1)}Al_{0.11(1)}Si_{0.94(2)}O_{3.03(1)}. A sample, MAOS3265, was a single crystal bridgmanite synthesized in an MA at 25 GPa and 1673 K (Figs. S1b and S2c) and then loaded into DAC for a series of SMS experiments. Another sample, DACMSRd01, was a polycrystalline bridgmanite directly synthesized from the gel in a DAC at 80 GPa and 2500 K (Figs. S1a and S2a). Mössbauer spectra of MAOS3265 were obtained at pressures of 50 and 14 GPa, and those of DACMSRd01 were obtained at pressures of 80, 50, and 12 GPa (Fig. 2). Before the SMS experiments at 50 and 80 GPa, we performed laser thermal annealing at about 2000 K and 2500 K, respectively, to release deviatoric stress in both samples (Table S1).

Results

The Mössbauer spectrum of MAOS3265 bridgmanite at 14 GPa was well fitted by two Lorentz-type doublets, corresponding to Fe²⁺ having higher center shift (CS) and quadrupole splitting (QS) values (Fe²⁺ #1) than Fe³⁺ (Fe³⁺ #1) (Fig. 2b). These components showed negligible differences with increasing pressure to 50 GPa, with CS and QS values of 0.94(13) and 2.39(32) (Fe²⁺ #1) and 0.33(12) and 1.38(28) mm/s (Fe³⁺ #1), respectively (Fig. 3 and Table S2). We assigned these values, which were consistent with the reported hyperfine parameters, to high-spin (HS) Fe²⁺ and Fe³⁺^{14,21,38,39} in the A-site. A component with a high QS value (Fe²⁺ #2) was observed at 50 GPa, which was attributed to the Fe²⁺ in the distorted A site^{21,38,40} (Fig. 2a). We found no evidence of low-spin (LS) Fe³⁺ in our annealed MAOS3265 bridgmanite at 50 GPa, which is suggested to have a similar QS value as that of HS-Fe³⁺ but with relatively low CS value^{21,38,39}.

The spectrum of bridgmanite sample DACMSRd01 at 12 GPa was composed of two components that were similar to those of MAOS3265 bridgmanite at 14 GPa (Fig. 2b,e). However, spectra at the higher pressures 50 and 80 GPa required another component of Fe³⁺ #2 with a low CS (~0.05 mm/s) for satisfactory fitting, which is likely to be attributed to LS Fe³⁺ in the B site, as found in previous studies^{21,38,39} (Figs. 2c,d and 3). The relative area of the LS Fe³⁺ component slightly decreased from 19.2 to 16.4% with decompression from 80 to 50 GPa, where the calculated LS fractions of Fe³⁺ (LS Fe³⁺/ΣFe³⁺) were both ~40%. Note that we did not observe a drastic increase in QS along the spin crossover that was predicted in a theoretical study³⁴, which was also the case in

synthesized in an MA, at 25 GPa



synthesized in a DAC from gel, at 80 GPa

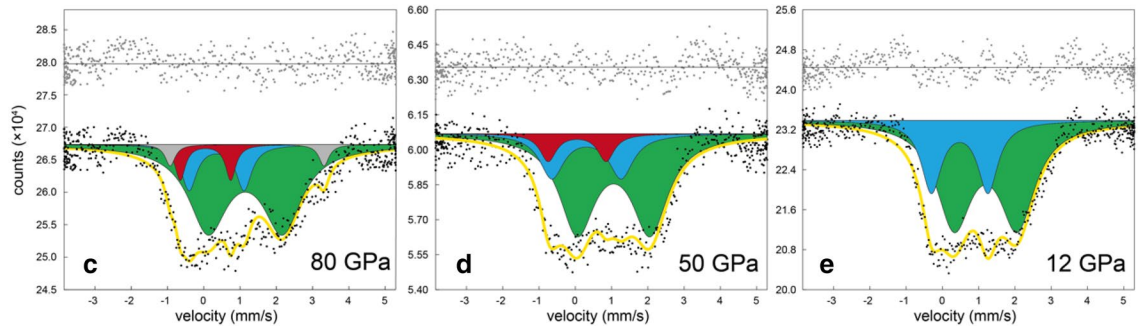


Figure 2. Evolution of the obtained SMS spectra of bridgmanite samples with decreasing pressure. (**a,b**) Bridgmanite synthesized in an MA at 25 GPa and 1673 K (MAOS3265) at 50 and 14 GPa, respectively, and (**c–e**) bridgmanite synthesized in a DAC at 80 GPa and 2500 K (DACMSRd01) at 80, 50, and 12 GPa, respectively. Green, grey, light blue, and red doublets indicate the components Fe^{2+} #1, Fe^{2+} #2, Fe^{3+} #1, and Fe^{3+} #2, respectively. Yellow curves show the theoretical fit, and grey symbols indicate the residual.

previous experimental studies^{38,39}. The pressure dependence of the $\text{Fe}^{3+}/\Sigma\text{Fe}$ ratio in each bridgmanite sample was nearly constant throughout the experiment (Fig. S4), which is an expected result since we avoided thermal annealing during decompression except at the highest-pressure data points of 50 and 80 GPa for MAOS3265 and DACMSRd01 bridgmanite, respectively.

Discussion

The present results at 50 GPa showed that bridgmanite synthesized at 25 GPa in an MA did not undergo the Fe^{3+} HS-LS spin transition, while bridgmanite formed directly from the amorphous starting material at 80 GPa in a DAC experienced the transition. We view our results for MAOS3265 bridgmanite in the following manner: when a single-crystal sample is used, i.e., under chemical composition-fixed conditions, the cation exchange reaction Eq. (1) is required for Fe^{3+} to be incorporated into the B site, but the reaction's large kinetic barrier^{20,21,25,42} hampers achieving the equilibrated site configuration and thus the accommodation of LS Fe^{3+} even with further pressurization and annealing; on the other hand, the chemical composition and cation configuration of the DAC-MSRd01 sample were equilibrated since a direct synthesis of bridgmanite in a DAC at high pressure where Fe^{3+} is stable in the LS state does not require the cation exchange in Eq. (1) to accommodate LS Fe^{3+} , which is consistent with the large LS fraction of Fe in bridgmanite formed in only a DAC at high pressure²⁵. Our results sufficiently explain the decade of conflicting studies of the reported spin state of Fe in bridgmanite^{13–29} (Figure S8). Still, it is noted that this is inconsistent with a consensus made by theoretical studies that FeAlO_3 is always energetically preferable to AlFeO_3 ^{31–34} (see Supplementary S6 for further discussion). The electrical conductivity and the thermal conductivity of (Fe, Al)-bearing bridgmanite-dominant rocks that accompanied the Fe spin transition are all synthesized at relatively high pressure (> 45 GPa) in a DAC^{27,43}, while those without it were synthesized in a MA^{23,44}. The contradictory studies of the electrical conductivity^{43,44} and the thermal conductivity^{23,27} of (Fe, Al)-bearing bridgmanite-dominant rocks can also be explained by our results.

An SMS experiment on (Fe,Al)-bearing glass at room T with a similar chemical composition used in the present study did not show a spin transition⁴⁵, indicating the importance of the thermal process or crystallization of bridgmanite for hosting LS-Fe in the SiO_6 octahedra. We should note that glass with a substantial amount of Fe and Al such as $\text{Fe}_3\text{Al}_2\text{Si}_3\text{O}_{12}$ ⁴⁶ and MORB composition⁴⁷ are reported to contain LS-Fe without thermal process, which is still under debate and may be due to difference in chemical composition. The amorphous starting material is a good proxy of melt^{47–50}, and we can expect bridgmanite crystallized from melt to have the same inheritance of the Fe spin state as in our study.

The density relationship among the forming minerals and the residual melts and their thermophysical properties govern the lower mantle dynamics. Our findings add information on the spin state of bridgmanite to the proposed evolution scenarios. The density and viscosity contrast between primordial material and pyrolite is

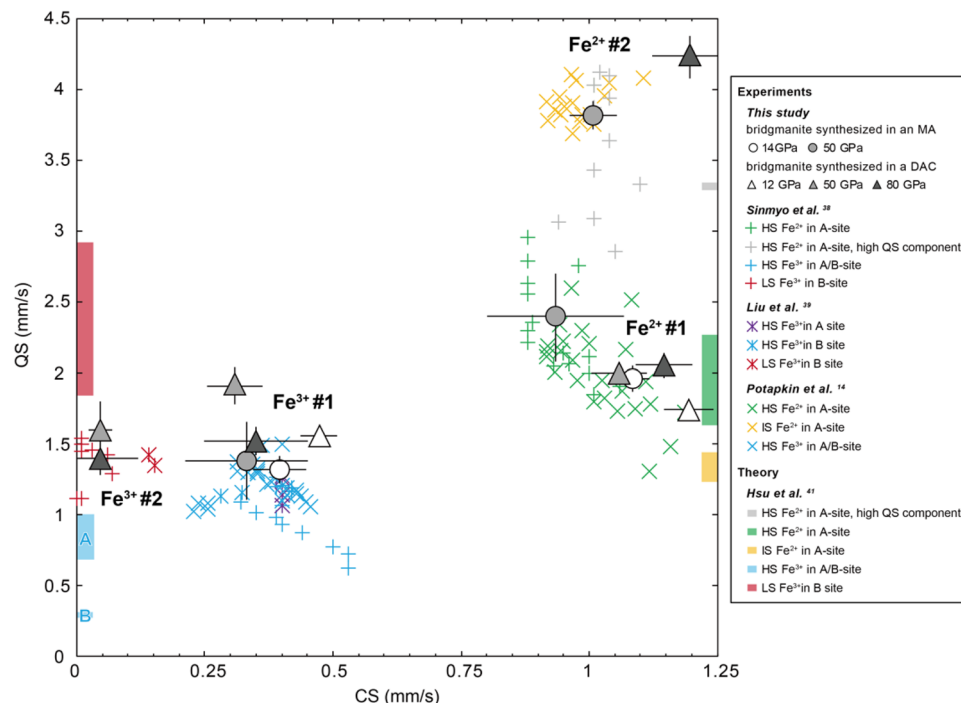


Figure 3. Mössbauer parameters of bridgmanite. Triangles, bridgmanite synthesized in a DAC (this study); circles, bridgmanite synthesized in an MA (this study). The reported Mössbauer parameters of bridgmanite are also plotted as a reference: plus symbols, Sinmyo et al.³⁸; stars, Liu et al.³⁹; crosses, Potapkin et al.¹⁴, respectively. The differences in colours represent the differences in assigned sites in previous studies: green, grey, yellow, light blue, and red symbols indicate the Mössbauer parameters assigned to HS Fe²⁺ in the A site, HS Fe²⁺ in the A site with a high QS component, intermediate-spin (IS) Fe²⁺ in the A site, HS Fe³⁺ in the A/B site, and LS Fe³⁺ in the B site, respectively. Density functional theory results for Fe³⁺ are shown on the left, and those for Fe²⁺ are shown on the right⁴¹.

suggested to enhance the preservation of primordial material⁹, which is robustly predicted from geochemical evidence^{10,11}. A density contrast of more than ~0.4% seems to be required to preserve primordial domains during the long-term evolution of the Earth⁹, including a large blob primordial domain such as the bridgmanite-enriched ancient mantle structures (BEAMS)⁸. A HS-to-LS transition of Fe³⁺ in bridgmanite can result in a stronger density contrast (Supplementary S5); the spin transition of 10 mol% Fe³⁺ in bridgmanite causes ~0.6(2)% densification⁵¹, which favours a mantle convection model that preserves primordial material until today. Although the effect of the spin transition of Fe in bridgmanite on its viscosity is unknown, the second major lower mantle mineral, ferropericlase, shows a viscosity maximum at the depth corresponding to the onset pressure of the HS-to-LS transition of Fe of 40 GPa⁵². The viscosity of bridgmanite may behave similarly to that of ferropericlase. However, temperature is thought to enhance the spin transition pressure and widens the pressure interval^{53,54}, which should weaken the effect of Fe spin transition in bridgmanite on its elasticity and viscosity than expected. We should also be aware that the temperature conditions in our study (~2500 K) covers most of the present mantle geotherm, but that of the early Earth's mantle is thought to be much higher (~3500 K) so that the observed LS fraction of Fe³⁺ in bridgmanite may be different from that in early mantle bridgmanite. Since higher temperature enhances the stability field of HS⁵³, verification along with quantitative data from high *P*-*T* experiments is required for further discussion.

Our study suggests that bridgmanite crystallized from the deep magma ocean contains LS Fe³⁺, whose effect on mantle dynamics has never been considered. The evolution and dynamics of the deeper part of the Earth's lower mantle may have been controlled by the “denser” Fe,Al-bearing bridgmanite for over billions of years from the freezing stage of the magma ocean to the present.

Methods

Preparation of bridgmanite samples. The gel starting material was synthesized at the Tokyo Institute of Technology. The gel starting material was heated at 727 °C in a H₂-CO₂ gas-mixing furnace in which oxygen fugacity (*f*O₂) was controlled to be slightly above the iron-wüstite (IW) buffer (Supplementary S2). The chemical composition of the starting material was determined to be Mg_{0.78(3)}Fe_{0.13(1)}Al_{0.11(1)}Si_{0.94(2)}O_{3.03(1)} by electron probe microanalyzer (EPMA) JXA-8530F in Tokyo Institute of Technology. ⁵⁷Fe-enriched Fe powder (⁵⁷Fe/total Fe ~ 96%) was used in the synthesis of the gel for high-pressure Mössbauer spectroscopy measurements.

The MAOS3265 sample was synthesized using a 2000-ton Kawai-type MA apparatus (ORANGE-2000) at Ehime University. The gel starting material was heated at 1000 °C in a H₂-CO₂ gas-mixing furnace to synthesize

enstatite in which fO_2 was controlled to be slightly above the IW buffer. The phase was identified by a micro section XRD measurement using Rigaku RAPID II-V/DW to be single-phase clinoenstatite (Fig. S2b). This was packed into a Re foil capsule and then loaded into a MgO container. In the synthesis experiment using the MA apparatus, an (Mg,Co)O octahedral pressure medium with an edge length of 10 mm and 8 tungsten carbide anvils with a truncation edge length of 4 mm were employed. Heating was performed for 2 h at 25 GPa and 1673 K, respectively, using a LaCrO₃ heater. The synthesis temperature was monitored with a W3Re-W25Re thermocouple. As a result, we obtained an almost single-phase bridgmanite that was confirmed by XRD measurement using a Rigaku RAPID II-V/DW (Fig. S2c). The chemical composition was determined to be Mg_{0.88(1)}Fe_{0.13(1)}Al_{0.11(1)}Si_{0.91(1)}O_{2.98(1)} by EPMA. A single crystal was polished to a disk (~30 × 30 × 15 μm³) and loaded into a sample chamber in a DAC with a pressure medium of KCl, whose culet size was 300 μm (Fig. S1b). The pressure was determined from a Raman spectrum of the diamond anvil⁵⁵. We used a typical value of 10% for pressure errors.

The disk-shaped gel starting material (~25 × 25 × 4 μm³) had gold sputtered on both sides as a laser absorber and was loaded into the sample chamber with a pressure transmitting medium of Al₂O₃ (Fig. S1a). The chemical composition of the sample in our previous studies with the use of Al₂O₃ pressure medium has never altered from that of the starting material^{27,28}. The chemical composition of our bridgmanite sample before and after the experiment was analysed by EPMA JXA-8530F in the Tokyo Institute of Technology. We found that the chemical composition did not change before and after the experiment (Supplementary S1). Double-sided laser heating was conducted at BL10XU, SPring-8 to synthesize bridgmanite sample DACMSRd01. The size of the laser spot was larger than the sample size, and the entire gel starting material was converted into bridgmanite. Simultaneously, in situ XRD measurements were conducted to identify the crystalline phase with a 30 keV incident X-ray (Fig. S2a). We used a pair of bevelled diamonds with a culet size of 120 μm.

Synchrotron Mössbauer spectroscopy at BL10XU, SPring-8. In situ high-pressure synchrotron Mössbauer spectroscopy measurements were all performed at BL10XU, SPring-8⁵⁶. The X-ray energy was set to 14.4125 keV using double monochromatic Si(111) crystals, and the energy around the nuclear resonance energy of ⁵⁷Fe was tuned using a high-resolution monochromator (HRM) consisting of nested-type channel-cut Si(511) and Si(975) crystals. A ⁵⁷FeBO₃ single-crystal heated to the Néel temperature in a 160 G external magnetic field was used for the nuclear monochromator, in which Bragg reflection (333) produced ultrafine monochromatic X-rays with an energy bandwidth of ~15 neV (calculated from the instrumental function) and an absorber bandwidth of 95% ⁵⁷Fe-enriched K₂MgFe(CN)₆ of 0.197 mm/s. The ⁵⁷FeBO₃ crystal was mounted on a velocity transducer and operated in sinusoidal velocity mode. A NaI scintillation detector was used to count the ⁵⁷Fe Mössbauer radiation. The collection time of the Mössbauer spectra was 4.5–16 h for each signal (Table S1). All measurements were carried out upon decompression from the highest pressure in each run. The obtained Mössbauer absorption spectra were fitted using a full transmission integral fit with Lorentzian-squared line shape using the MossA software package⁵⁷.

Received: 31 May 2021; Accepted: 15 September 2021

Published online: 30 September 2021

References

- Elkins-Tanton, L. T. Linked magma ocean solidification and atmospheric growth for Earth and Mars. *Earth Planet. Sci. Lett.* **271**, 181–191 (2008).
- Nakajima, M. & Stevenson, D. J. Melting and mixing states of the Earth's mantle after the Moon-forming impact. *Earth Planet. Sci. Lett.* **427**, 286–295 (2015).
- Canup, R. M. Forming a moon with an earth-like composition via a giant impact. *Science* **338**, 1052–1055 (2012).
- Lock, S. J. *et al.* The origin of the moon through a terrestrial synestia. *J. Geophys. Res. Planets* **123**, 910–951 (2018).
- Ito, E., Kubo, A., Katsura, T. & Walter, M. J. Melting experiments of mantle materials under lower mantle conditions with implications for magma ocean differentiation. *Phys. Earth Planet. Inter.* **143**, 397–406 (2004).
- Tateno, S., Hirose, K. & Ohishi, Y. Melting experiments on peridotite to lowermost mantle conditions. *J. Geophys. Res. Solid Earth* **119**, 4684–4694 (2014).
- Xie, L. *et al.* Formation of bridgmanite-enriched layer at the top lower-mantle during magma ocean solidification. *Nat. Commun.* **11**, 1–10 (2020).
- Ballmer, M. D., Houser, C., Hernlund, J. W., Wentzcovitch, R. M. & Hirose, K. Persistence of strong silica-enriched domains in the Earth's lower mantle. *Nat. Geosci.* **10**, 236–240 (2017).
- Gülcher, A. J. P., Gebhardt, D. J., Ballmer, M. D. & Tackley, P. J. Variable dynamic styles of primordial heterogeneity preservation in the Earth's lower mantle. *Earth Planet. Sci. Lett.* **536**, 116160 (2020).
- Mundl, A. *et al.* Tungsten-182 heterogeneity in modern ocean island basalts. *Science* **356**, 66–69 (2017).
- Hyung, E. & Jacobsen, S. B. The ¹⁴²Nd/¹⁴⁴Nd variations in mantle-derived rocks provide constraints on the stirring rate of the mantle from the Hadean to the present. *Proc. Natl. Acad. Sci. U. S. A.* **117**, 14738–14744 (2020).
- Badro, J. *et al.* Electronic transitions in perovskite: Possible nonconvecting layers in the lower mantle. *Science* **305**, 383–386 (2004).
- Ballaran, T. B. *et al.* Effect of chemistry on the compressibility of silicate perovskite in the lower mantle. *Earth Planet. Sci. Lett.* **333–334**, 181–190 (2012).
- Potapkin, V. *et al.* Effect of iron oxidation state on the electrical conductivity of the Earth's lower mantle. *Nat. Commun.* **4**, 4–9 (2013).
- Glazyrin, K. *et al.* Magnesium silicate perovskite and effect of iron oxidation state on its bulk sound velocity at the conditions of the lower mantle. *Earth Planet. Sci. Lett.* **393**, 182–186 (2014).
- Ismailova, L. *et al.* Stability of Fe, Al-bearing bridgmanite in the lower mantle and synthesis of pure Fe-bridgmanite. *Sci. Adv.* **2**, e1600427 (2016).

17. Lin, J. F. *et al.* High-spin Fe²⁺ and Fe³⁺ in single-crystal aluminous bridgmanite in the lower mantle. *Geophys. Res. Lett.* **43**, 6952–6959 (2016).
18. Mao, Z. *et al.* Equation of state and hyperfine parameters of high-spin bridgmanite in the Earth's lower mantle by synchrotron X-ray diffraction and Mössbauer spectroscopy. *Am. Mineral.* **102**, 357–368 (2017).
19. Li, J. *et al.* Electronic spin state of iron in lower mantle perovskite. *Proc. Natl. Acad. Sci. U. S. A.* **101**, 14027–14030 (2004).
20. Fujino, K. *et al.* Spin transition of ferric iron in Al-bearing Mg-perovskite up to 200 GPa and its implication for the lower mantle. *Earth Planet. Sci. Lett.* **317–318**, 407–412 (2012).
21. Kuppenko, I. *et al.* Oxidation state of the lower mantle: In situ observations of the iron electronic configuration in bridgmanite at extreme conditions. *Earth Planet. Sci. Lett.* **423**, 78–86 (2015).
22. Zhu, F. *et al.* Synthesis, elasticity, and spin state of an intermediate MgSiO₃-FeAlO₃ Bridgmanite: Implications for iron in earth's lower mantle. *J. Geophys. Res. Solid Earth* **125**, 1–11 (2020).
23. Okuda, Y. *et al.* The effect of iron and aluminum incorporation on lattice thermal conductivity of bridgmanite at the Earth's lower mantle. *Earth Planet. Sci. Lett.* **474**, 25–31 (2017).
24. Nishio-Hamane, D., Seto, Y., Fujino, K. & Nagai, T. Effect of FeAlO₃ incorporation into MgSiO₃ on the bulk modulus of perovskite. *Phys. Earth Planet. Inter.* **166**, 219–225 (2008).
25. Catalli, K. *et al.* Effects of the Fe³⁺ spin transition on the properties of aluminous perovskite—New insights for lower-mantle seismic heterogeneities. *Earth Planet. Sci. Lett.* **310**, 293–302 (2011).
26. Shim, S. H. *et al.* Stability of ferrous-iron-rich bridgmanite under reducing midmantle conditions. *Proc. Natl. Acad. Sci. U. S. A.* **114**, 6468–6473 (2017).
27. Okuda, Y. *et al.* Effect of spin transition of iron on the thermal conductivity of (Fe, Al)-bearing bridgmanite. *Earth Planet. Sci. Lett.* **520**, 188–198 (2019).
28. Okuda, Y., Ohta, K., Sinmyo, R., Hirose, K. & Ohishi, Y. Anomalous compressibility in (Fe, Al)-bearing bridgmanite: implications for the spin state of iron. *Phys. Chem. Miner.* **47**, 40 (2020).
29. Dorfman, S. M. *et al.* Effects of composition and pressure on electronic states of iron in bridgmanite. *Am. Mineral.* **105**, 1030–1039 (2020).
30. Lin, J. F., Speziale, S., Mao, Z. & Marquardt, H. Effects of the electronic spin transitions of iron in lower mantle minerals: Implications for deep mantle geophysics and geochemistry. *Rev. Geophys.* **51**, 244–275 (2013).
31. Caracas, R. Elasticity of AlFeO₃ and FeAlO₃ perovskite and post-perovskite from first-principles calculations. *Geophys. Res. Lett.* **37**, 3–7 (2010).
32. Mohn, C. E. & Trønnes, R. G. Iron spin state and site distribution in FeAlO₃-bearing bridgmanite. *Earth Planet. Sci. Lett.* **440**, 178–186 (2016).
33. Shukla, G., Cococcioni, M. & Wentzcovitch, R. M. Thermoelasticity of Fe³⁺- and Al-bearing bridgmanite: Effects of iron spin crossover. *Geophys. Res. Lett.* **43**, 5661–5670 (2016).
34. Hsu, H., Yu, Y. G. & Wentzcovitch, R. M. Spin crossover of iron in aluminous MgSiO₃ perovskite and post-perovskite. *Earth Planet. Sci. Lett.* **359–360**, 34–39 (2012).
35. Ballmer, M. D., Lourenço, D. L., Hirose, K., Caracas, R. & Nomura, R. Reconciling magma-ocean crystallization models with the present-day structure of the Earth's mantle. *Geochem. Geophys. Geosyst.* **18**, 2785–2806 (2017).
36. Labrosse, S., Hernlund, J. W. & Coltice, N. A crystallizing dense magma ocean at the base of the Earth's mantle. *Nature* **450**, 866–869 (2007).
37. Caracas, R., Hirose, K., Nomura, R. & Ballmer, M. D. Melt-crystal density crossover in a deep magma ocean. *Earth Planet. Sci. Lett.* **516**, 202–211 (2019).
38. Sinmyo, R., McCammon, C. & Dubrovinsky, L. The spin state of Fe³⁺ in lower mantle bridgmanite. *Am. Mineral.* **102**, 1263–1269 (2017).
39. Liu, J. *et al.* Valence and spin states of iron are invisible in Earth's lower mantle. *Nat. Commun.* **9**, 1–9 (2018).
40. McCammon, C. *et al.* Stable intermediate-spin ferrous iron in lower-mantle perovskite. *Nat. Geosci.* **1**, 684–687 (2008).
41. Hsu, H., Blaha, P., Cococcioni, M. & Wentzcovitch, R. M. Spin-state crossover and hyperfine interactions of ferric iron in MgSiO₃ perovskite. *Phys. Rev. Lett.* **106**, 1–4 (2011).
42. Zhu, F. *et al.* Synthesis, elasticity, and spin state of an intermediate MgSiO₃-FeAlO₃ bridgmanite: Implications for Iron in earth's lower mantle. *J. Geophys. Res. Solid Earth* **125**, e19964 (2020).
43. Ohta, K. *et al.* Electrical conductivities of pyrolytic mantle and MORB materials up to the lowermost mantle conditions. *Earth Planet. Sci. Lett.* **289**, 497–502 (2010).
44. Sinmyo, R., Pesce, G., Greenberg, E., McCammon, C. & Dubrovinsky, L. Lower mantle electrical conductivity based on measurements of Al, Fe-bearing perovskite under lower mantle conditions. *Earth Planet. Sci. Lett.* **393**, 165–172 (2014).
45. Mao, Z. *et al.* Spin and valence states of iron in Al-bearing silicate glass at high pressures studied by synchrotron Mossbauer and X-ray emission spectroscopy. *Am. Mineral.* **99**, 415–423 (2014).
46. Dorfman, S. M. *et al.* Electronic transitions of iron in almandine-composition glass to 91 GPa. *Am. Mineral.* **101**, 1659–1667 (2016).
47. Murakami, M. *et al.* High-pressure radiative conductivity of dense silicate glasses with potential implications for dark magmas. *Nat. Commun.* **5**, 1–6 (2014).
48. Williams, Q. & Jeanloz, R. Spectroscopic evidence for pressure-induced coordination changes in silicate glasses and melts. *Science* **239**, 902–905 (1988).
49. Lee, S. K. *et al.* X-ray Raman scattering study of MgSiO₃ glass at high pressure: Implication for triclustered MgSiO₃ melt in Earth's mantle. *Proc. Natl. Acad. Sci. USA* **105**, 7925–7929 (2008).
50. Allwardt, J. R. *et al.* Effect of structural transitions on properties of high-pressure silicate melts: ²⁷Al NMR, glass densities, and melt viscosities. *Am. Mineral.* **92**, 1093–1104 (2007).
51. Mao, Z., Lin, J. F., Yang, J., Inoue, T. & Prakapenka, V. B. Effects of the Fe³⁺ spin transition on the equation of state of bridgmanite. *Geophys. Res. Lett.* **42**, 4335–4342 (2015).
52. Deng, J. & Lee, K. K. M. Viscosity jump in the lower mantle inferred from melting curves of ferropericlase. *Nat. Commun.* **8**, 1997 (2017).
53. Tsuchiya, T. & Wang, X. Ab initio investigation on the high-temperature thermodynamic properties of Fe³⁺-bearing MgSiO₃ perovskite. *J. Geophys. Res. Solid Earth* **118**, 83–91 (2013).
54. Shukla, G. & Wentzcovitch, R. M. Spin crossover in (Mg, Fe³⁺)(Si, Fe³⁺)O₃ bridgmanite: Effects of disorder, iron concentration, and temperature. *Phys. Earth Planet. Inter.* **260**, 53–61 (2016).
55. Akahama, Y. & Kawamura, H. High-pressure Raman spectroscopy of diamond anvils to 250 GPa: Method for pressure determination in the multimegabar pressure range. *J. Appl. Phys.* **96**, 3748–3751 (2004).
56. Hirao, N. *et al.* New developments in high-pressure X-ray diffraction beamline for diamond anvil cell at SPring-8. *Matter Radiat. Extrem.* **5**, 018403 (2020).
57. Prescher, C., McCammon, C. & Dubrovinsky, L. MossA: A program for analyzing energy-domain Mössbauer spectra from conventional and synchrotron sources. *J. Appl. Crystallogr.* **45**, 329–331 (2012).

Acknowledgements

We thank two anonymous reviewers for their helpful comments. We acknowledge Prof. E. Ohtani for instrumental support, Dr. I. Mashino for data analysis, and Prof. K. Hirose for helpful discussion. A bridgmanite sample was synthesized at the Geodynamic Research Center, Ehime University, under the PRIUS program (Project No. 2017-B07). The synchrotron Mössbauer spectroscopy measurements were conducted at BL10XU, SPring-8 (proposal no. 2017B1730, 2019B1740). This work was supported by JSPS KAKENHI Grant Number JP15H05827.

Author contributions

K.O. and Yo.O. designed the study and wrote the manuscript. Yo.O. carried out most of the experiments and was helped by Y.N., N.H., S.I., Ya.O., S.S., and T.W. Yo.O. and T.W. analysed the data. All authors discussed the results and commented on the manuscript.

Competing interests

The authors declare no competing interests.

Additional information

Supplementary Information The online version contains supplementary material available at <https://doi.org/10.1038/s41598-021-98991-w>.

Correspondence and requests for materials should be addressed to Y.O.

Reprints and permissions information is available at www.nature.com/reprints.

Publisher's note Springer Nature remains neutral with regard to jurisdictional claims in published maps and institutional affiliations.



Open Access This article is licensed under a Creative Commons Attribution 4.0 International License, which permits use, sharing, adaptation, distribution and reproduction in any medium or format, as long as you give appropriate credit to the original author(s) and the source, provide a link to the Creative Commons licence, and indicate if changes were made. The images or other third party material in this article are included in the article's Creative Commons licence, unless indicated otherwise in a credit line to the material. If material is not included in the article's Creative Commons licence and your intended use is not permitted by statutory regulation or exceeds the permitted use, you will need to obtain permission directly from the copyright holder. To view a copy of this licence, visit <http://creativecommons.org/licenses/by/4.0/>.

© The Author(s) 2021